Effect of adiabatic index on Richtmyer-Meshkov flows induced by strong shocks

Cameron E. Wright and Snezhana I. Abarzhi

Abstract Richtmyer-Meshkov Instability (RMI) is an instability that develops at the interface between fluids of contrasting densities when impacted by a shock wave. Its applications include inertial confinement fusion, supernovae explosions, and the evolution of blast waves. We systematically study the effect of the adiabatic index of the fluids on the dynamics of strong-shock driven flows, particularly the amount of shock energy available for interfacial mixing. Only limited information is currently available about the dynamic properties of matter at these extreme regimes. Smooth Particle Hydrodynamics simulations are employed to ensure accurate shock capturing and interface tracking. A range of adiabatic indexes is considered, approaching limits which, to the best of the author's knowledge, have never been considered before. We analyse the effect of the adiabatic indexes on the interface speed and growth-rate immediately after the shock passage. The simulation results are compared, wherever possible, with rigorous theories and with experiments, achieving good quantitative and qualitative agreement. We find that the more challenging cases for simulations arise where the adiabatic indexes are further apart, and that the initial growth rate is a non-monotone function of the initial perturbation amplitude, which holds across all adiabatic indexes of the fluids considered. The applications of these findings on experiment design are discussed.

1 Introduction

Richtmyer-Meshkov instability (RMI) is a phenomenon in fluid mechanics that describes the evolution of an interface between two fluids of distinct acoustic impedance and distinct densities when a shock wave impacts the interface. The flow evolution is shown in **Figure 1**, where the light (red) fluid travels with velocity to-

Snezhana I. Abarzhi
School of Mathematics and Statistics, The University of Western Australia
e-mail: snezhana.abarzhi@gmail.com

wards the interface (light green) and heavy fluid (blue) and the Richtmyer-Meshov instability develops as the interface between the two fluids changes shape and size over time. ([Richtmyer, 1960]; [Meshkov, 1969]). If the interface between the fluids is given an initial perturbation a_0, (seen on the right in **Figure 1**) the interface amplitude increases in size with growth-rate v_0 as the wave travels and evolves into a large-scale coherent structure of bubbles and spikes (bottom right of **Figure 1**) ([Abarzhi, 2010]; [Abarzhi, 2008]).

1.1 Motivation

Richtmyer-Meshkov instability (RMI) appears in a variety of processes in high energy density plasmas, controlling fluid transformation under strong impact, governing the formation of hot spots in inertial confinement fusion, determining energy transport in core-collapse supernova, and strongly influences the evolution of blast waves and explosions ([Meshkov, 1969]; [Richtmyer, 1960]). RMI forms in situations characterized by strong impact shocks, sharply and quickly changing flow fields, and by small effects of dissipation and diffusion, often producing small scale structures ([Abarzhi, 2010]). Interaction of a shock wave with a density discontinuity such as in the situation in this work may result in the development of RMI and in extensive interfacial mixing ([Meshkov, 1969]; [Richtmyer, 1960]). Since RMI plays such a large role in these applications, the ability to understand and control this instability is very important.

To the best of the author's knowledge, previous numerical simulations investigating the dynamics of RMI flows have only contained ideal monotonic gases. This study aims to investigate RMI flows for gases with more than one atom per molecule, e.g. diatomic or triatomic gases such as O_2 or H_2O. This is significant for investigation, as it will enable RMI studies to have a wider field of application as it will be able to more accurately model situations with high-speed non-monatomic gases, and aid in control of the instability through the initial parameter set-up. The applications include rocket thrust flow (such as those in scramjets), inertial confinement fusion, and explosion blast waves ([Drake, 2009]; [Bodner et al., 1998]; [Zel'dovich, 1967]).

1.2 Approach

Sometimes, in applications such as inertial confinement fusion, the effects of the Richtmyer-Meshkov instability are undesirable, and it is necessary to control the instability's evolution ([Lindl et al., 2004]). Some methods of achieving this include suppressing RMI completely, or controlling it through adjusting the initial parameters of the system ([Anisimov et al., 2013]; [Abarzhi, 2010]; [Demskoĭ et al., 2006]). In order to do this, information is required about the effect the initial parameters

have on the development of the instability. Of particular interest in controlling the development of the instability is the amount of energy available for interfacial mixing deposited into the interface from the shock wave. This is one of the aims of this study.

The volume of physical experimental data of RMI produced by strong shocks is sparse as the experiments require challenging control of flow implementation and diagnostics. ([Motl et al., 2009]; [Orlicz et al., 2009]; [Jacobs and Krivets, 2005]). Therefore, numerical modeling of RMI is a powerful tool to aid in designing and building systems in which RMI is present. However, the dynamics of RMI are complex and a numerical model should be able to manage numerous competing requirements, such as shock capturing, interface tracking, and accurate accounting for the dissipation processes ([Stanic et al., 2012]; [McFarland et al., 2011]; [Herrmann et al., 2008]; [Dimonte et al., 2004]).

Using a hydrodynamic approximation, we systematically study a broad spectrum of the parameter regime and its influence on the fraction of energy available for interfacial mixing in RM flow. To do this, we will obtain data on three variables of the flow- the interface speed, the interface growth rate, and the initial curvature of the front of the interface. These variables inform us to how much mixing of the interface occurs, and how well the numerical simulations capture small scale structures, which the simulations must do well in order to obtain data on the interfacial mixing. The results of each of these variables are compared with rigorous theoretical theories, finding good quantitative and qualitative agreement.

1.3 RMI Dynamics

RMI develops when a shock impacts an interface between two fluids of differing densities and the energy is distributed throughout the fluids ([Aleshin et al., 1990]). This dissertation will only focus on 2 dimensional RMI case, and with the shock propagating from the light fluid into the heavy fluid. When the shock hits an ideally planar interface (without any perturbation), it splits into a reflected shock travelling back through the light fluid and a transmitted shock travelling through the heavy fluid ([Stanic et al., 2012]; [Herrmann et al., 2008]; [Demskoĭ et al., 2006]). The bulk of the fluid influenced by the shock impact (the bulk between the reflected shock and the transmitted shock, including the fluid interface) all moves with the same velocity v_∞, called the background velocity, seen in **Figure 1**.

The velocity v_∞ quantifies the amount of energy transferred into the fluid bulk by the shock and is a function of the shock strength and fluid properties ([Stanic et al., 2012]; [Richtmyer, 1960]).

If the interface between the two fluids is perturbed (no longer planar), the bulk fluid containing the interface still moves with velocity v_∞, but the interface itself now has growth-rate v_0 due to the impulsive acceleration induced by the shock ([Meshkov, 1969]; [Richtmyer, 1960]). Arrows mark the direction of fluid motion at the tip of the bubble (right) and spike (left). Eventually, the bubble and spike

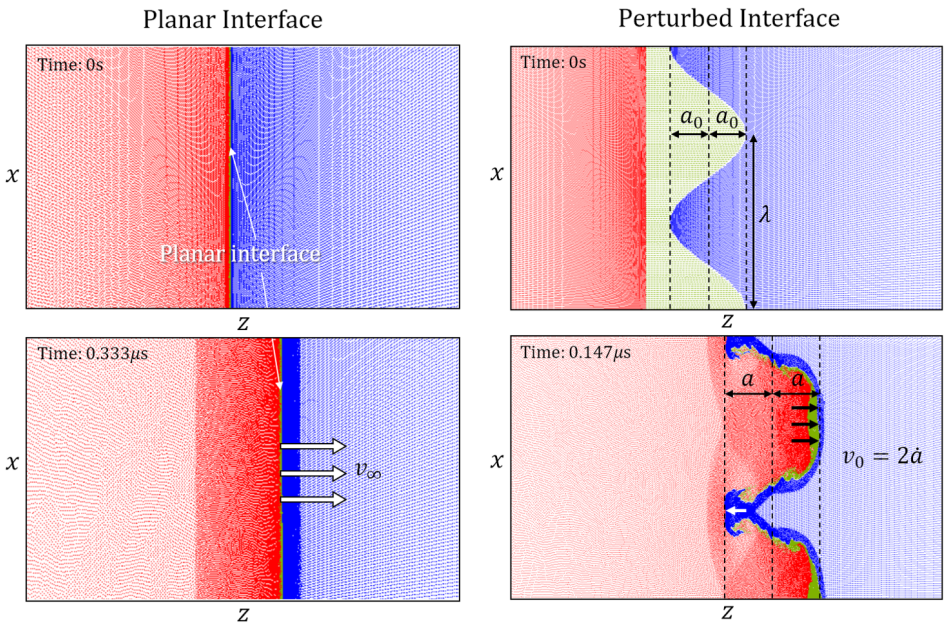

Fig. 1 Evolution of the Richtmyer-Meshkov instability for both the planar interface and perturbed interface cases. In both cases, the interface moves at speed v_∞, and the interface also grows with speed v_0 in the perturbed interface case, whereas it stays flat in the planar interface case.

growth decelerates, and small scale structures appear on the sides of the developing spikes ([Stanic et al., 2012]).

1.4 Parameters of the System

1.4.1 Mach Number

The Mach number, denoted M, is defined as the ratio of the speed of a shock to the speed of sound in the light fluid $c_l = 2.039 \times 10^3$m/s ([Richtmyer, 1960]). For weak shocks, $M \approx 1$, the background motion (the motion of the whole body of fluid) is subsonic relative to the light fluid, $v_\infty/c_l < 1$, where c_l is the speed of sound in the light fluid. For $M \approx 3$ the ratio is $v_\infty/c_l \approx 1$. For shocks with $M \approx 5$ the background motion is supersonic, $v_\infty/c_l > 1$, and for shocks with $M > 7$, the background motion is hypersonic, $v_\infty/c_l \gg 1$ ([Stanic et al., 2013]; [Stanic et al., 2012]; [Herrmann et al., 2008]).

1.4.2 Atwood Number

The Atwood number, denoted A, describes the density difference between two adjacent fluids with a common interface.

$$A = \frac{\rho_h - \rho_l}{\rho_h + \rho_l} \tag{1.4.1}$$

where ρ_h, ρ_l are the densities of the heavy and light fluids respectively.

1.4.3 Adiabatic Index

The adiabatic index of a substance, denoted γ, can be understood from three perspectives. From a thermodynamic point of view, the adiabatic index gives an important relation for an adiabatic process of an ideal gas:

$$PV^{\gamma} = \text{constant} \tag{1.4.2}$$

where P, V, and γ is the pressure, volume, and adiabatic index respectively of the fluid.

It can also be understood as the ratio of the heat capacity at constant pressure C_P to the heat capacity at constant volume C_V,

$$\gamma = \frac{C_P}{C_V}. \tag{1.4.3}$$

From a molecular dynamics point of view, the adiabatic index can also be related to the degrees of freedom f of a molecule as

$$\gamma = 1 + \frac{2}{f}. \tag{1.4.4}$$

To the best of the author's knowledge, previous simulation analyses of the dynamics of RMI flows have been conducted with an adiabatic index of $\gamma = 5/3$, which is the value for ideal monotonic gases. Its value decreases for gases with more than one atom per molecule, e.g. for diatomic gases $\gamma = 7/5$. While γ is known to have a strong influence on the flow dynamics, no systematic study has been undertaken on the effect of γ on the dynamics. The gases analysed in this study are theoretical ones, where we vary the adiabatic index of the heavy and light fluids systematically instead of choosing particular gases.

1.5 Parameter Regime

The parameter regime we investigate is for the Mach and Atwood numbers, $(M, A) = (5, 0.8)$. This pair has been well documented in previous studies ([Stanic et al., 2012];

[Dell et al., 2015]). We vary the adiabatic index of the heavy and light fluid $(\gamma_l, \gamma_h) = (1.2, 1.3, \cdots, 1.6)$. For each pair of γ_l and γ_h, the amplitude of the initial perturbation of the interface between the two bulk fluids was varied from 0% to 100% of the interface wavelength, ie $a_0/\lambda = (0, 0.1, 0.2, \ldots, 1)$ where a_0 is the amplitude of the sinisoidal initial perturbation, and λ is the wavelength of the perturbation. This is a well studied regime, and has been documented well in the past, allowing us to compare our results with previous studies ([Dell et al., 2015]; [Stanic et al., 2012]; [Stanic et al., 2013]).

This regime contains 275 cases, and we ran a numerical simulation for each case. The average simulation takes 36 hours to run, making a total of about 10,000 hours. The simulations were run on three Windows laptop computers with i7 processors and with 8GB, 12GB, and 16GB of RAM.

2 Methods

2.1 Theoretical Approaches

In this work, we compare the results from our numerical simulations to analytical solutions. This analysis takes different forms depending on the progression of the instability. In the initial linear regime of RMI, the interface perturbation grows at a constant rate v_0, which is a function of the amplitude a_0 and wavelength λ of the initial perturbation ([Richtmyer, 1960]). In the following nonlinear regime, the interface perturbation growth-rate decreases and a large coherent structure of spikes and bubbles appears ([Abarzhi, 2010]; [Abarzhi, 2008]). The heavy fluid penetrates the light fluid in spikes as seen on the bottom right of **Figure 1**. As they travel, the spikes decelerate and small scale structures form on the sides of the spikes ([Stanic et al., 2012]).

2.1.1 Zeroth-order theory

An important parameter of RMI dynamics is v_∞, the magnitude of the velocity (hereafter: velocity) of the bulk, or the background motion. This value can be precisely calculated by zeroth-order theory from the conditions of the conservation of mass, momentum, and energy, and the equations of state of the fluids ([Richtmyer, 1960]). For ideal gases, it is a function of the initial shock's Mach number, the adiabatic index of the fluids $\gamma_{h(l)}$, and the Atwood number, $v_\infty = v_\infty(M, A, \gamma_{h(l)})$, and it is useful because it quantifies the amount of energy deposited by the shock into the fluid bulk ([Stanic et al., 2012]). The analysis of the numerical simulations becomes much simpler once v_∞ is obtained and used as the characteristic time scale so that the frame of reference is moving at speed v_∞ ([Dell et al., 2015]).

2.1.2 Linear theory

Another important parameter in RMI dynamics is the initial growth-rate v_0 of the interface. It is a function of M, A, $\gamma_{h(l)}$, and the initial perturbation amplitude and wavelength, $v_0 = v_0(M, A, \gamma_{h(l)}, a_0, \lambda)$ ([Stanic et al., 2012]; [Nishihara et al., 2010]; [Holmes et al., 1999]). For very small amplitude ($a_0/\lambda = 10^{-2}$ or smaller), v_0 is precisely calculated by linear theory, and grows linearly with a_0, $v_0 \approx \frac{a_0}{\lambda} M c_l$ ([Nishihara et al., 2010]; [Wouchuk, 2001]; [Richtmyer, 1960]).

For moderately small values of a_0, the growth rate v_0 becomes non-linear and has been calculated in previous studies by [Velikovich et al., 2014]; [Nishihara et al., 2010], and [Velikovich and Dimonte, 1996]. For larger values of a_0, the rate v_0 may grow with a_0 even slower than the linear and weakly nonlinear theory predict ([Stanic et al., 2012]; [Holmes et al., 1999]).

2.1.3 Highly nonlinear theory

In the late stages of Richtmyer-Meshkov dynamics v_0 has been calculated with group theory consideration ([Abarzhi, 2010]; [Abarzhi et al., 2003]; [Abarzhi, 2002]). At this late stage, the bubbles decelerate and flatten, and there is almost no fluid motion away from the interface, and extensive interfacial mixing occurs ([Stanic et al., 2013]; [Stanic et al., 2012]; [Herrmann et al., 2008]). These late-time dynamics are a complex problem, and many features require better understanding.

2.2 Smoothed Particle Hydrodynamics Simulations

Numerical modelling of RMI in these extreme conditions is a difficult task because the method should be able to accurately handle large speeds, strong shocks, and preserve small scale structures with high precision and accuracy. These small scale structures are embedded in large scale dynamics, moving at high speeds, so the order of precision required is very large ([Anisimov et al., 2013]). To model these complex dynamics we have employed the Smoothed Particle Hydrodynamics code (SPHC), which is an open-source code written in C developed by Dr. Stellingwerf and has free access to a complete set of validation test cases ([Stellingwerf, 1991]). This code has been widely used and tested on a broad variety of shock and flow problems, including RMI dynamics, the Noh problem, and with problems involving plasmas, complex materials, and multiphase flows ([Stanic et al., 2013]; [Stanic et al., 2012]; [Monaghan, 2005]; [Lucy, 1977]; [Stellingwerf, 1990]). Particularly, it has been used by NASA to investigate the Space Shuttle Columbia incident ([Stellingwerf et al., 2004]). SPHC conserves momentum, angular momentum, mass, and energy globally and locally and reflects particles on the boundaries in order to produce the correct boundary solutions, accurate to within 0.001% ([Stellingwerf, 1990]).

2.2.1 SPH Technique

SPH is a grid-free method that represents a continuous fluid with fixed-mass SPH particles, which are each represented by a mathematical basis function (or kernel) ([Stellingwerf, 1990]). In essence, SPHC keeps track of a large array of particles and for each time step, and calculates each interaction between all particles.

2.2.2 SPHC Simulation Setup

In this study, the computational setup is the standard similar to that in [Stanic et al., 2012] in order to extend the results of previous studies.

The amplitude is set at the start of every run, and when the shock hits the interface, the interface amplitude is compressed and then grows as RMI develops. We want to obtain the initial growth-rate of the interface, so we locate the first minimum of the amplitude and take v_0 to be the slope of the linear regression line from the first minimum amplitude over the next few initial data points, as seen in **Figure 2**. Note that v_0 is defined as the time derivative of the difference of the initial positions of the bubble and spike, which is twice the amplitude, as in [Stanic et al., 2012].

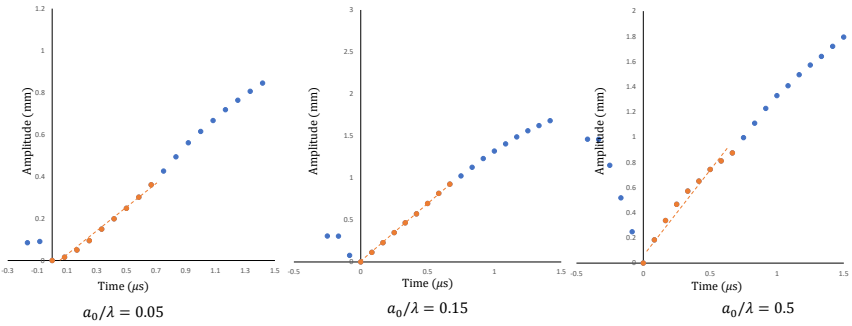

Fig. 2 The method by which v_0 is measured. We take the gradient of the the data points where $0 < t < 0.8\tau$ (marked in orange). The cases displayed are for $\gamma_l = 1.5$, $\gamma_h = 1.5$.

However, an issue arises when choosing what data points to include, because the value of v_0 changes significantly depending on where the cutoff for the initial growth is defined. To solve this problem, we notice that the shape of the amplitude-time curve for early time changes depending on the value of the initial perturbation, marked in orange in **Figure 2**. For $a_0/\lambda = 0.1$ the curve is concave, for $a_0/\lambda = (0.2, 0.3)$ the curve is linear, and for $a_0/\lambda = (0.4, 0.5, \cdots, 1)$ the curve is convex, forming a bubble like shape. Each of these shapes have clearly defined endpoints, marked on the diagram by the first blue points: the first finishes at the inflection point (the transition from concave to convex), the second where the growth starts to become non linear, and the third finishes at the end of the convex "bubble" (and

where the second bubble begins). These endpoints for all three shapes all finish at 0.8τ, where $\tau = v_\infty/\lambda$, giving $0.8\tau = 6.67 \times 10^{-7}$. These patterns are consistent across all different values of $\gamma_{h(l)}$ and a_0/λ considered, and this method produces good results, which indicates that this is a good choice.

To find v_∞, we measure the speed of the interface in the ideally planar interface case, with $a_0/\lambda = 1 \times 10^{-12} \approx 0$ (which is the smallest perturbation the simulation software would allow). The position of the interface is taken to be the leftmost position of the interface, as in [Dell et al., 2015]. The planar interface position motion is almost perfectly linear in time, allowing very accurate calculation of v_∞ by taking the slope of the linear regression line of the interface position over time. When the interface is not planar, the growth of the interface interferes with the measurement of the speed of the bulk, making accurate measurements difficult. However, because the amplitude of the interface doesn't affect the speed of the bulk, the values of v_∞ calculated for the planar case are taken to be the same for cases where $a_0/\lambda \neq 0$ ([Dell et al., 2015]).

3 Results

3.1 Background Motion for Planar Interface Case

Using the SPHC simulations and the method described above, we calculated the value of v_∞ for the cases $(M,A) = (5, 0.8)$, with γ_h and γ_l ranging from $1.2, 1.3, \cdots,$ 1.6. The results of these calculations are shown in **Figure 3**. The shape of the curves formed for each γ_h value when γ_l ranges from 1.2 to 1.6 appears to be decreasing in a non-linear fashion, which may be approaching a value asymptotically. In order to determine the behaviour accurately, more data points are required and may need further investigation in future studies.

We compare these results to the analytical calculations produced by zero-order theory [Richtmyer, 1960], where v_∞ can be calculated precisely from zero-order theory in the planar interface case (when the initial perturbation is 0) ([Stanic et al., 2012]; [Richtmyer, 1960]). The percentage error between the simulation results and the zero-order theory is shown in **Table 1**.

γ_l \ γ_h	1.2	1.3	1.4	1.5	1.6
1.2	0.641	4.87	9.52	12.9	16.7
1.3	5.75	0.732	3.56	7.54	10.5
1.4	9.75	4.87	0.597	-2.79	5.68
1.5	12.8	8.04	4.00	0.822	-2.15
1.6	15.3	10.5	6.74	3.68	0.836

Table 1 Percentage error for v_∞ calculated from the SPHC simulations for the cases $a_0/\lambda = 0, \gamma_l, \gamma_h = (1.2, 1.3, \cdots, 1.6)$ when compared to the zero-order theory predictions. Values with high error ($> 7\%$) are marked in red.

We found that when gamma heavy and gamma light are close, simulation agreement with the linear series is close- <7%. Values with errors above these thresholds are marked in red. In particular, when $\gamma_l = \gamma_h$, the agreement is excellent, $> 99\%$.

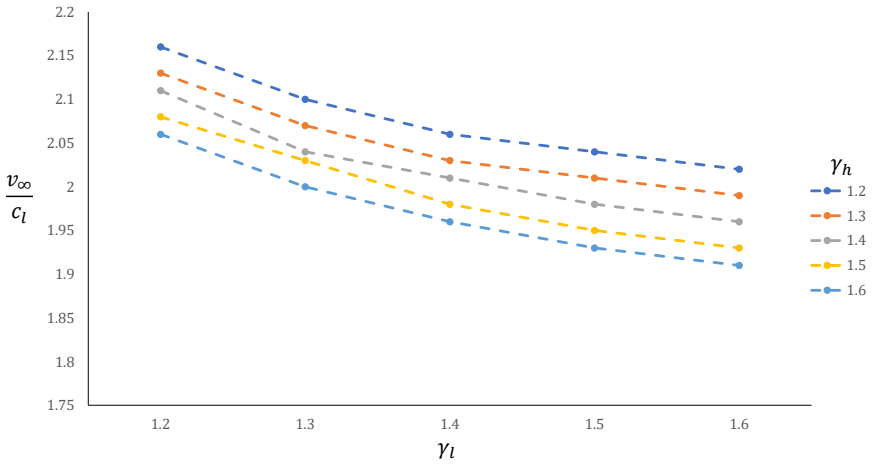

Fig. 3 Plot of v_∞/c_l for values of γ_l (on the x axis) and γ_h (coloured data points)

We found that if γ_l and γ_h are too different with $\gamma_{h(l)} \geq \gamma_{l(h)} + 2$ for $\gamma_{l(h)} = (1.2, 1.3)$ or $\gamma_{h(l)} \geq \gamma_{l(h)} + 3$ for $\gamma_{l(h)} = (1.4, 1.5, 1.6)$, the simulations don't handle those situations well and the results are too inaccurate to make predictions and are excluded from further simulation analysis in this work. To the best of the author's knowledge, this observation has not been made before, and may prove useful in the understanding of scenarios with varying adiabatic indexes.

γ_l \ γ_h	1.2	1.3	1.4	1.5	1.6
1.2	0.432	0.426			
1.3	0.421	0.414	0.409		
1.4		0.406	0.402	0.396	0.391
1.5			0.396	0.391	0.386
1.6			0.393	0.387	0.382

Table 2 Results for $v_\infty/(M \cdot c_l)$ for each value of γ_l and γ_h with $a_0/\lambda = 0$. Values with error >7% are excluded.

Table 2 shows the results for v_∞, scaled by c_l and M, the speed of sound in the light fluid and the Mach number, respectively. We see that the velocity of the background motion, v_∞ is only a fraction of the shock velocity, ranging from ∼20% to ∼40%.

3.2 Initial Amplitude Growth Rate for Perturbed Interface

3.2.1 Simulation Results

After the shock passes through the interface, the interface amplitude grows approximately linearly with time, as we see in **Figure 2**. When this value is calculated from the simulations, we scale it by the velocity of the bulk fluid, v_∞, which is done to compare the interface growth rate to the background motion. This value v_0/v_∞ quantifies the distribution of the energy imparted by the shock wave between the interfacial fluid and the bulk fluid ([Dell et al., 2015]).

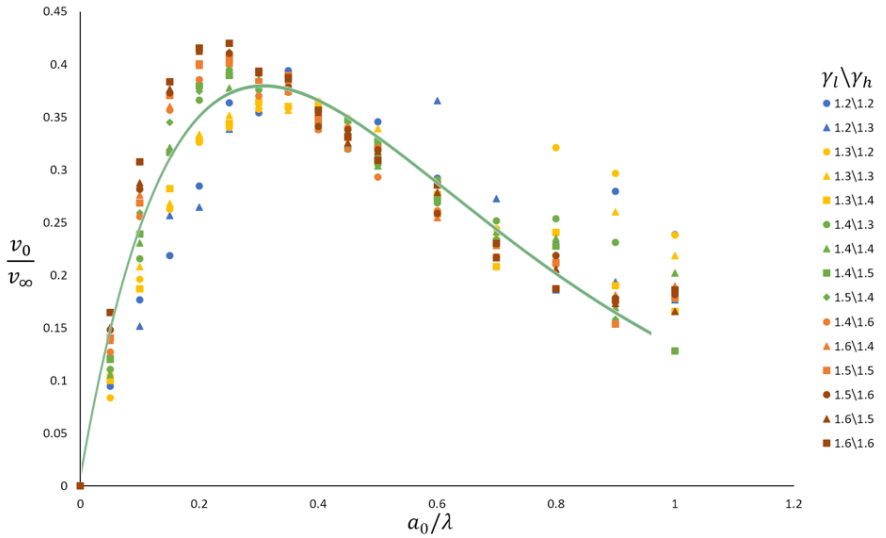

Fig. 4 Plot of v_0/v_∞ against a_0/λ with an approximate curve fitted.

We ran simulations for $(M,A) = (5,0.8), \gamma_l, \gamma_h = (1.2, 1.3, \ldots, 1.6)$, and $a_0/\lambda = (0, 0.1, 0.2 \ldots, 1)$. Determining the interface amplitude growth-rate v_0 and bulk velocity v_∞ from the simulations using the method as described in Section 2.2.2, we plot their ratio v_0/v_∞ for each value of a_0/λ, displayed in **Figure 4**. A well-defined shape is formed, which increases linearly for early time, becomes non linear and eventually peaks and decreases for late time, asymptotically approaching 0. As in [Abarzhi et al., 2019]; [Dell et al., 2017], and [Dell et al., 2015], a function satisfying these criteria is

$$\frac{v_0}{v_\infty} \cdot \frac{1}{A} = c_1 \cdot \frac{a_0}{\lambda} \cdot e^{-c_2 \cdot \frac{a_0}{\lambda}}. \tag{3.2.1}$$

This depends on the Atwood number and two constants, c_1 and c_2. Our objective is to ascertain how well the simulation data fits this curve and to find these constants to compare them with linear theory and to assess the accuracy of our simulations.

Letting $x = \frac{a_0}{\lambda}$ and $y = \frac{v_0}{v_\infty} \cdot \frac{1}{A}$, we have

$$y = c_1 x e^{-c_2 x}. \tag{3.2.2}$$

As we see in **Figure 4**, the curve follows the data closely.

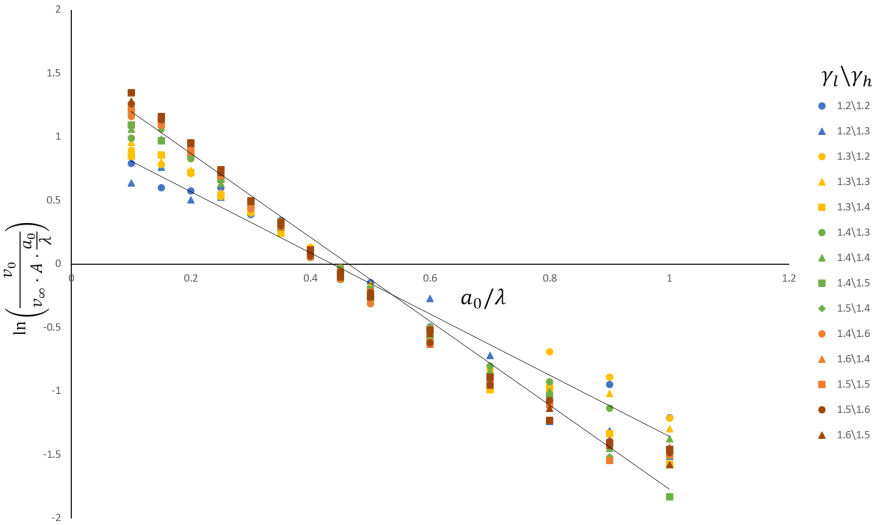

Fig. 5 The combined calculated values of v_0/v_∞ for all pairs of γ_l and γ_h linearised according to the proposed equation that describes their behaviour with a linear regression line fitted.

To determine the constants c_1 and c_2 of the equation of the curve and to quantify the strength of the relationship between the data and the curve, we rearrange Equation 3.2.2 to form a linear relationship so that a linear regression line can be fitted to the data:

$$\begin{aligned} y &= c_1 x e^{-c_2 x} \\ \frac{y}{c_1 x} &= e^{-c_2 x} \\ \ln\left(\frac{y}{c_1 x}\right) &= -c_2 x \\ \ln\left(\frac{y}{x}\right) - \ln(c_1) &= -c_2 x \\ \ln\left(\frac{y}{x}\right) &= (-c_2)x + \ln c_1 \end{aligned} \tag{3.2.3}$$

Letting $\hat{y} = \ln\left(\frac{y}{x}\right), m = -c_2, n = \ln(c_1)$, we have the linear relation

$$\hat{y} = m \cdot x + n. \tag{3.2.4}$$

c_1						c_2					
γ_l \ γ_h	1.2	1.3	1.4	1.5	1.6	γ_l \ γ_h	1.2	1.3	1.4	1.5	1.6
1.2	2.88	2.76				1.2	2.36	2.27			
1.3	3.39	3.53	3.46			1.3	2.78	2.87	2.86		
1.4		4.28	4.45	4.40	5.00	1.4		3.40	3.47	3.39	3.80
1.5			4.86	5.18	5.40	1.5			3.67	3.81	3.90
1.6			5.21	5.51	5.80	1.6			3.82	3.95	4.09

Table 3 Values of c_1 and c_2 for each value of γ_l and γ_h in our parameter regime.

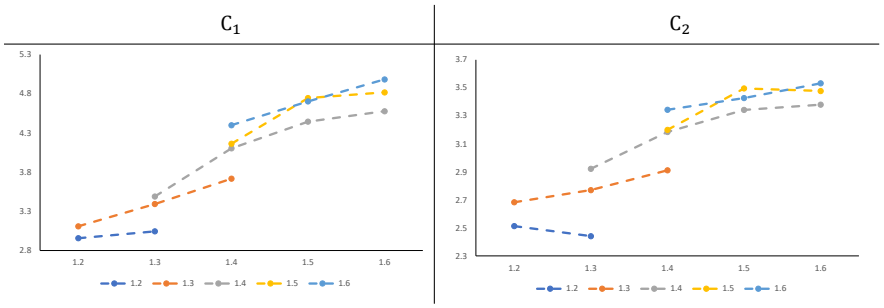

Fig. 6 Plots of c_l and c_2 for values of γ_l (on the x axis) and γ_h (coloured data points)

We plot $\hat{y}$ against x for all chosen values of γ_l, γ_h (excluding those found to produce high errors) and for $a_0/\lambda = (0.1, 0.2, \cdots, 1)$. The plot of all the values of γ_h and γ_l combined is shown in **Figure 5**, where the relationship can be seen to be strongly negative and linear. The value of c_1 is calculated by taking the exponential of the y-intercept of the linear regression line, m, and c_2 is the negative of the slope of the line, n, which follows from the setup of Equation 3.2.2. The values of c_1 and c_2 for each pair of γ_l, γ_h are calculated from the lines of best fit in **Figure 5**, and are shown in **Table 3**.

The plot of the results of the constants c_1 and c_2 is shown in **Figure 6**. These plots reveal some information about the variation in the constants with respect to γ_l and γ_h. Both values of c_1 and c_2 have roughly the same shapes, but with $c_1 > c_2$. Higher values of γ_h produce higher values of c_1 and c_2. We see a linear increase in c_1 and c_2 for small γ_l, which becomes slower than linear for higher values of γ_l.

We found that if we ordered the adiabatic indexes from small γ_h and γ_l to large γ_h and γ_l in a "diagonal" fashion (shown in **Figure 7**), we notice a trend in the values of c_1 and c_2. They appear to increase in a linear fashion, which to the best of

the author's knowledge has not been discussed before, and may benefit from future study.

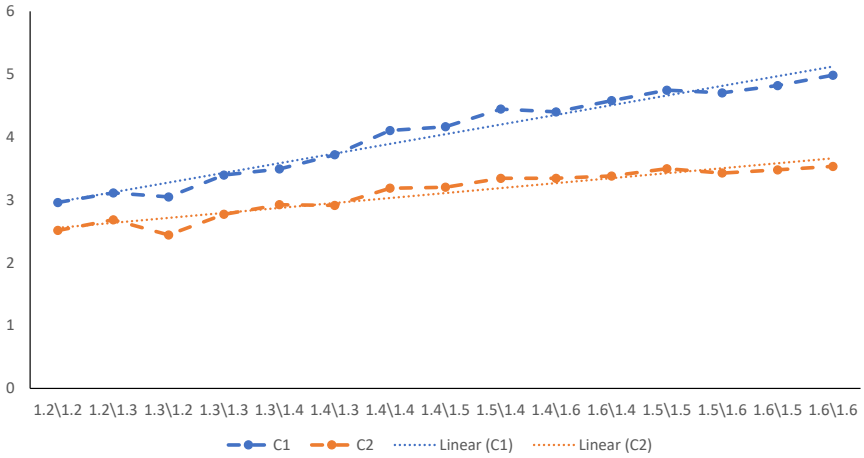

Fig. 7 Plot of the values of c_1 and c_2 for the ordered values of γ_l and γ_h. The equation of the c_1 line is $y = 0.1539x + 2.8127$, and the equation of the c_2 line is $y = 0.0791x + 2.4754$

3.2.2 Comparison of Simulation Results with Linear Theory

For small a_0/λ, $a_0/\lambda \leq 0.1$, the initial growth rate v_0 linearly depends on a_0. Linear theory can predict this growth for these small amplitudes, as seen in **Figure 8** ([Dell et al., 2015]). We compare this linear theory with our simulation results. Restating our equation relating interface growth rate and initial perturbation amplitude, we have

$$\frac{1}{A} \cdot \frac{v_0}{v_\infty} = c_1 \cdot \frac{a_0}{\lambda} \cdot e^{-c_2 \cdot \frac{a_0}{\lambda}}. \tag{3.2.5}$$

The linear theory finds values of $v_0/(v_\infty \cdot \frac{a_0}{\lambda})$ for small a_0/λ, so we choose the smallest initial amplitude, $a_0/\lambda = 0.1 \ll 1$. We rearrange Equation 3.2.5 to get

$$\left[\frac{v_0}{v_\infty \cdot \frac{a_0}{\lambda}}\right]_T = A \cdot c_1 \cdot e^{-0.1c_2}, \tag{3.2.6}$$

where $[\cdot]_T$ is the value obtained from the linear theory. The values of the theoretical $\left[\frac{v_0}{v_\infty \cdot \frac{a_0}{\lambda}}\right]_T$ are compared to the simulation data $A \cdot c_1 \cdot e^{-0.1c_2}$ in **Table 4**, as well as the percentage error. The simulation results are in good agreement with the theoretical values, with an average error of 4.68%. Only one of the fifteen cases

have an error of more than 10%, making this a very accurate prediction. In order to investigate the linear approximation more closely, we ran simulations over a finer increment of a_0/λ, increasing by 0.05 instead of 0.1, as displayed in **Figure 8**. The approximations for linear theory assume the perturbation amplitude to be very small, $ka_0 \ll 1$ or $a_0/\lambda < 0.05$, but we see that the approximation holds for larger amplitudes, up to $a_0/\lambda < 0.1$, which is a result consistent with previous studies ([Dell et al., 2017]; [Dell et al., 2015]).

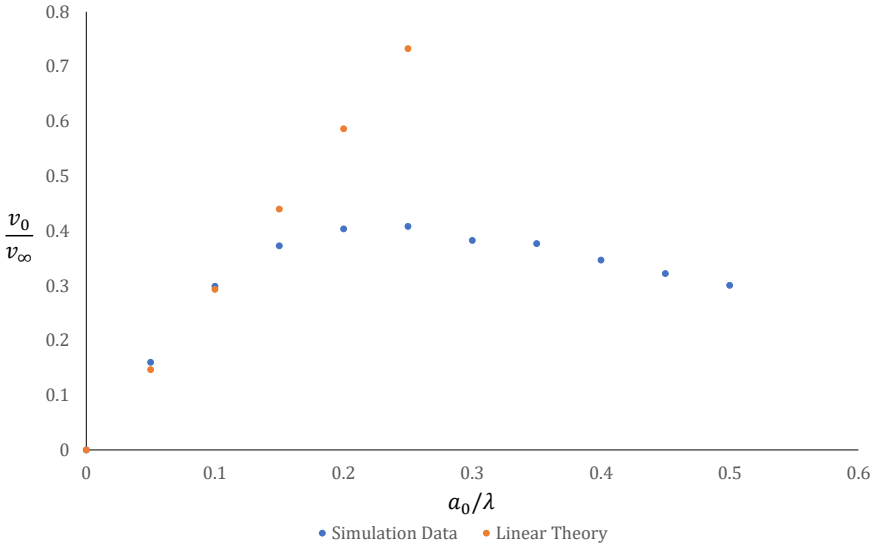

Fig. 8 Plot showing values of v_0/v_∞ from the simulations (blue), and the prediction from linear theory (orange). We see that linear theory only has predicting power for values of $a_0/\lambda \leq 0.1$.

3.2.3 Maximum Interface Growth-Rate

Of interest in experiments is the amount of energy that can be deposited into the interface by the shock, which determines the amount of energy available for interfacial mixing, discussed in **Section 3.3**. The maximum scaled interface growth rate v_0/v_∞ quantifies this amount, so is of interest in this study. We have found in **Section 3.2.1** that the interface growth-rate is a non-monotone function of the initial perturbation amplitude, and is described by the relationship

$$\frac{v_0}{v_\infty \cdot A} = c_1 \frac{a_0}{\lambda} e^{-c_2 \cdot \frac{a_0}{\lambda}}. \tag{3.2.7}$$

Letting $x = \frac{a_0}{\lambda}$ and $y = \frac{v_0}{v_\infty} \cdot \frac{1}{A}$, we have

	γ_l \ γ_h	1.2	1.3	1.4	1.5	1.6
Simulation	1.2	1.82	1.76			
	1.3	2.05	2.12	2.08		
	1.4		2.44	2.51	2.51	2.74
	1.5			2.69	2.83	2.92
	1.6			2.84	2.97	3.08
	γ_l \ γ_h	1.2	1.3	1.4	1.5	1.6
Theoretical	1.2	1.88	2.07			
	1.3	2.01	2.24	2.39		
	1.4		2.35	2.52	2.64	2.72
	1.5			2.62	2.75	2.84
	1.6			2.69	2.83	2.93
	γ_l \ γ_h	1.2	1.3	1.4	1.5	1.6
Error (%)	1.2	3.34	15.2			
	1.3	2.05	5.45	13.0		
	1.4		3.60	0.37	4.83	0.63
	1.5			2.72	3.20	2.88
	1.6			5.56	4.80	5.25

Table 4 Comparison of the values of $\frac{v_0}{v_\infty a_0/\lambda}$ from the linear theory and the simulation results, obtained using Equation 3.2.6.

$$y = c_1 x e^{-c_2 x}. \tag{3.2.8}$$

We find the maximum scaled interface growth rate $[v_0/v_\infty]_{max}$, from the data in **Section 3.2.1**. In order to find the a_0/λ at this maximum, we find where the gradient of Equation 3.2.8 is zero,

$$\begin{aligned} y'(x) &= c_1 e^{-c_2 x} - c_1 c_2 x e^{-c_2 x} = 0 \\ 0 &= c_1 - c_1 c_2 x \\ x &= \frac{1}{c_2}. \end{aligned} \tag{3.2.9}$$

The results for the maximum growth rate and the value of a_0/λ at which this maximum occurs are plotted in **Figure 9**. The plots range the adiabatic indexes from small γ_h and γ_l to large γ_h and γ_l in a "diagonal" fashion because it is easier and simpler to display the data in this way, and because we noticed a trend in the data when displayed in this fashion. This trend has not been discussed before, and may benefit from future study. The maximum growth rate hits a minimum at $(\gamma_l, \gamma_h) \approx (1.3, 1.4)$ before increasing in a linear fashion as (γ_l, γ_h) ranges to $(1.6, 1.6)$. The amplitude a_0/λ at which these occur decreases as γ_l, γ_h increases. The value v_0/v_∞ quantifies the fraction of energy imparted into the interface by the shock, and these results show that on average, $\sim 45\%$ of the bulk velocity is available for interfacial mixing. From **Table 2** we know that at on average $\sim 30\%$ of the shock velocity is imparted into the bulk motion, meaning that on average, only $\sim 15\%$ of the shock velocity is

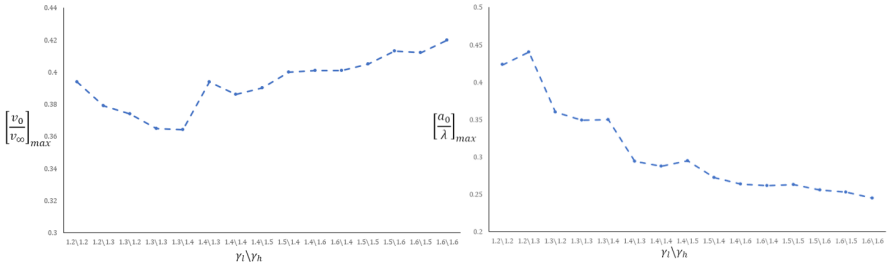

Fig. 9 Plots showing the maximum scaled interface growth-rate (top) and the initial perturbation amplitude at which this occurs (bottom) for all cases of γ_l and γ_h, arranged from lowest $\gamma_{h(l)}$ to highest $\gamma_{h(l)}$.

available for interfacial mixing. Despite this very small scale of mixing, our results are in good agreement with the theory, demonstrating the ability of SPHC to capture small scale dynamics embedded in large scale dynamics very accurately.

3.3 Discussion and Conclusion

In this study, through use of numerical simulations we have systematically studied the effect of a previously unconsidered regime of adiabatic indexes of the fluids on the early time dynamics of RMI, specifically the extent of the interfacial mixing. The key properties of the dynamics we have analysed are the velocity, growth-rate, and curvature of the interface. Our regime included the Mach and Atwood numbers, $(M,A) = (5,0.8)$, a range of adiabatic indexes $\gamma_l, \gamma_h = (1.2, 1.3, \cdots, 1.6)$ and a range of initial perturbations from 0% to 100% of the wavelength. In this regime, the simulations are repeatable and qualitatively similar, and we found good quantitative and qualitative agreement between the simulation results and the theory, demonstrating the accuracy at which SPHC simulations are able to capture small scale dynamics embedded within large scale dynamics in extreme and challenging situations.

In order to find the appropriate scale for the amount of energy deposited into the interface by the shock, we obtained the velocity of the background motion. In experiments, the background motion makes reliable diagnostics of RMI challenging because flow measurements must be taken from a quickly moving interface. Numerical simulations have the ability to scale the dynamics by the bulk velocity via the use of a Galilean transformation to a moving frame of reference. In order to scale our results, we obtained the bulk velocity v_∞ in **Section 3.1**, and we found that the more challenging cases for the simulations to model occur when the adiabatic indexes of the two fluids are further apart (**Table 1**), which to the best of the author's knowledge is the first time this observation has been made. To ensure our results were reliable, we removed the cases that were challenging for our simulations to model accurately from consideration.

In order to quantify the amount of energy deposited into the interface by the shock, we found the initial growth rate of the interface v_0, and scaled it by the velocity of the background motion v_∞. The speed at which the interface spreads out indicates how much energy the interface received from the initial shock. We found that the initial growth rate is a non-monotone function of the initial perturbation amplitude, and that this relationship is insensitive to the adiabatic indexes of the fluids (**Figure 4**). For each pair of adiabatic indexes, we found the maximum values of the growth-rate scaled by the background motion, v_0/v_∞, and at which values of a_0/λ this occurred. We found that this maximum changes with γ_l and γ_h (**Figure 9**). We found that on average, only $\sim 15\%$ of the shock velocity is transferred to the growth of the interface, indicating that only a fraction of the energy from the shock is deposited into the interface and is hence available for interfacial mixing. We compared our simulation results to linear theory, and found the average error to be less than 5% for the bulk velocity (**Table 1**) and the interface growth-rate (**Table 4**). This indicates that the SPHC simulations can handle small scale dynamics embedded in large scale dynamics with high accuracy.

Our results provide good benchmarks for further studies and experiments and open up further avenues of investigation for non-ideal adiabatic indexes. Our results also have implications for hydrodynamic instabilities and mixing in inertial confinement fusion (ICF). To achieve ICF ignition, the ability to avoid or control the Richtmyer-Meshkov instability that forms during the implosion process is necessary ([Lindl et al., 2004]). One method is to fully suppress the development of RMI, which is based on traditional scenarios of RMI that suggest that the development of RMI may produce uncontrolled growth of small-scale imperfections and lead to disordered mixing that is similar to canonical turbulence ([Dimonte et al., 2004]). However, research conducted in studies like this through simulations and theoretical analysis suggests that the interfacial mixing may keep a significant degree of order, shown by the ability to accurately predict the evolution of the interface through theoretical analysis. These findings suggest that the dynamics can be controlled through the initial perturbation, so that turbulent mixing may be prevented without having to completely suppress RMI, which may be easier to implement ([Dell et al., 2015]; [Anisimov et al., 2013]; [Abarzhi, 2010]; [Demskoĭ et al., 2006]). This study also suggests there is reason to have confidence in the ability of the numerical simulations produced by SPHC in accurately capturing small scale dynamics embedded in large scale structures despite its difficulty.

References

[Abarzhi, 2002] Abarzhi, S. (2002). A new type of the evolution of the bubble front in the Richtmyer–Meshkov instability. *Physics Letters A*, 294(2):95–100.

[Abarzhi, 2008] Abarzhi, S. (2008). Review of nonlinear dynamics of the unstable fluid interface: conservation laws and group theory. *Physica Scripta*, T132:014012.

[Abarzhi et al., 2003] Abarzhi, S., Nishihara, K., and Glimm, J. (2003). Rayleigh–Taylor and Richtmyer-Meshkov instabilities for fluids with a finite density ratio. *Physics Letters A*,

317(5):470–476.

[Abarzhi, 2010] Abarzhi, S. I. (2010). Review of theoretical modeling approaches of Rayleigh-Taylor instabilities and turbulent mixing. *Philosophical Transactions of the Royal Society A: Mathematical, Physical and Engineering Sciences*, 368(1916):1809–1828.

[Abarzhi et al., 2019] Abarzhi, S. I., Bhowmick, A. K., Naveh, A., Pandian, A., Swisher, N. C., Stellingwerf, R. F., and Arnett, W. D. (2019). Supernova, nuclear synthesis, fluid instabilities, and interfacial mixing. *Proceedings of the National Academy of Sciences*, 116(37):18184–18192.

[Aleshin et al., 1990] Aleshin, A. N., Lazareva, E. V., Zaitsev, S. G., Rozanov, V. B., Gamalii, E. G., and Lebo, I. G. (1990). Linear, nonlinear, and transient stages in the development of the Richtmyer-Meshkov instability. *Soviet Physics Doklady*, 35:159.

[Anisimov et al., 2013] Anisimov, S. I., Drake, R. P., Gauthier, S., Meshkov, E. E., and Abarzhi, S. I. (2013). What is certain and what is not so certain in our knowledge of Rayleigh-Taylor mixing? *Philosophical Transactions of the Royal Society A: Mathematical, Physical and Engineering Sciences*, 371(2003):20130266.

[Bodner et al., 1998] Bodner, S. E., Colombant, D. G., Gardner, J. H., Lehmberg, R. H., Obenschain, S. P., Phillips, L., Schmitt, A. J., Sethian, J. D., McCrory, R. L., Seka, W., Verdon, C. P., Knauer, J. P., Afeyan, B. B., and Powell, H. T. (1998). Direct-drive laser fusion: Status and prospects. *Physics of Plasmas*, 5(5):1901–1918.

[Dell et al., 2015] Dell, Z., Stellingwerf, R. F., and Abarzhi, S. I. (2015). Effect of initial perturbation amplitude on Richtmyer-Meshkov flows induced by strong shocks. *Physics of Plasmas*, 22(9):092711.

[Dell et al., 2017] Dell, Z. R., Pandian, A., Bhowmick, A. K., Swisher, N. C., Stanic, M., Stellingwerf, R. F., and Abarzhi, S. I. (2017). Maximum initial growth-rate of strong-shock-driven Richtmyer-Meshkov instability. *Physics of Plasmas*, 24(9):090702.

[Demskoĭ et al., 2006] Demskoĭ, D. K., Marikhin, V. G., and Meshkov, A. G. (2006). Lax representations for triplets of two-dimensional scalar fields of chiral type. *Teoret. Mat. Fiz.*, 148(2):189–205.

[Dimonte et al., 2004] Dimonte, G., Youngs, D. L., Dimits, A., Weber, S., Marinak, M., Wunsch, S., Garasi, C., Robinson, A., Andrews, M. J., Ramaprabhu, P., Calder, A. C., Fryxell, B., Biello, J., Dursi, L., MacNeice, P., Olson, K., Ricker, P., Rosner, R., Timmes, F., Tufo, H., Young, Y.-N., and Zingale, M. (2004). A comparative study of the turbulent Rayleigh–Taylor instability using high-resolution three-dimensional numerical simulations: The Alpha-Group collaboration. *Physics of Fluids*, 16(5):1668–1693.

[Drake, 2009] Drake, R. P. (2009). Perspectives on high-energy-density physics. *Physics of Plasmas*, 16(5):055501.

[Herrmann et al., 2008] Herrmann, M., Moin, P., and Abarzhi, S. I. (2008). Nonlinear evolution of the Richtmyer-Meshkov instability. *J. Fluid Mech.*, 612:311–338.

[Holmes et al., 1999] Holmes, R. L., Dimonte, G., Fryxell, B., Gittings, M. L., Grove, J. W., Schneider, M., Sharp, D. H., Velikovich, A. L., Weaver, R. P., and Zhang, Q. (1999). Richtmyer–Meshkov instability growth: experiment, simulation and theory. *Journal of Fluid Mechanics*, 389:55–79.

[Jacobs and Krivets, 2005] Jacobs, J. W. and Krivets, V. V. (2005). Experiments on the late-time development of single-mode Richtmyer-Meshkov instability. *Physics of Fluids*, 17(3):034105.

[Lindl et al., 2004] Lindl, J. D., Amendt, P., Berger, R. L., Glendinning, S. G., Glenzer, S. H., Haan, S. W., Kauffman, R. L., Landen, O. L., and Suter, L. J. (2004). The physics basis for ignition using indirect-drive targets on the National Ignition Facility. *Physics of Plasmas*, 11(2):339–491.

[Lucy, 1977] Lucy, L. B. (1977). A numerical approach to the testing of the fission hypothesis. *Astronomical Journal*, 82:1013–1024.

[McFarland et al., 2011] McFarland, J. A., Greenough, J. A., and Ranjan, D. (2011). Computational parametric study of a Richtmyer-Meshkov instability for an inclined interface. *Phys. Rev. E*, 84:026303.

[Meshkov, 1969] Meshkov, E. E. (1969). Instability of the interface of two gases accelerated by a shock wave. *Fluid Dynamics*, 4(5):101–104.

[Monaghan, 2005] Monaghan, J. J. (2005). Smoothed particle hydrodynamics. *Reports on Progress in Physics*, 68(8):1703–1759.

[Motl et al., 2009] Motl, B., Oakley, J., Ranjan, D., Weber, C., Anderson, M., and Bonazza, R. (2009). Experimental validation of a Richtmyer–Meshkov scaling law over large density ratio and shock strength ranges. *Physics of Fluids*, 21(12):126102.

[Nishihara et al., 2010] Nishihara, K., Wouchuk, J. G., Matsuoka, C., Ishizaki, R., and Zhakhovsky, V. V. (2010). Richtmyer-Meshkov instability: Theory of linear and nonlinear evolution. *Philosophical Transactions of the Royal Society A: Mathematical, Physical and Engineering Sciences*, 368(1916):1769–1807.

[Orlicz et al., 2009] Orlicz, G. C., Balakumar, B. J., Tomkins, C. D., and Prestridge, K. P. (2009). A Mach number study of the Richtmyer–Meshkov instability in a varicose, heavy-gas curtain. *Physics of Fluids*, 21(6):064102.

[Richtmyer, 1960] Richtmyer, R. D. (1960). Taylor instability in shock acceleration of compressible fluids. *Communications on Pure and Applied Mathematics*, 13(2):297–319.

[Stanic et al., 2013] Stanic, M., McFarland, J., Stellingwerf, R. F., Cassibry, J. T., Ranjan, D., Bonazza, R., Greenough, J. A., and Abarzhi, S. I. (2013). Non-uniform volumetric structures in Richtmyer-Meshkov flows. *Physics of Fluids*, 25(10):106107.

[Stanic et al., 2012] Stanic, M., Stellingwerf, R. F., Cassibry, J. T., and Abarzhi, S. I. (2012). Scale coupling in Richtmyer-Meshkov flows induced by strong shocks. *Physics of Plasmas*, 19(8):082706.

[Stellingwerf, 1991] Stellingwerf, B. (1991). Stellingwerf Consulting. www.stellingwerf.com.

[Stellingwerf et al., 2004] Stellingwerf, R., Robinson, J., Richardson, S., Evans, S., Stallworth, R., and Hovater, M. (2004). Foam on tile impact modeling for the STS-107 investigation. 5.

[Stellingwerf, 1990] Stellingwerf, R. F. (1990). *Smooth particle hydrodynamics*, chapter 25, pages 239–247. Springer Verlag.

[Velikovich and Dimonte, 1996] Velikovich, A. L. and Dimonte, G. (1996). Nonlinear perturbation theory of the incompressible Richtmyer-Meshkov instability. *Phys. Rev. Lett.*, 76:3112–3115.

[Velikovich et al., 2014] Velikovich, A. L., Herrmann, M., and Abarzhi, S. I. (2014). Perturbation theory and numerical modelling of weakly and moderately nonlinear dynamics of the incompressible Richtmyer-Meshkov instability. *Journal of Fluid Mechanics*, 751:432–479.

[Wouchuk, 2001] Wouchuk, J. G. (2001). Growth rate of the linear Richtmyer-Meshkov instability when a shock is reflected. *Phys. Rev. E*, 63:056303.

[Zel'dovich, 1967] Zel'dovich, I. B. (1967). *Physics of shock waves and high-temperature hydrodynamic phenomena*. Academic Press, New York.